

# Micrometer-Scale Porous Buckling Shell Actuators Based on Liquid Crystal Networks

Venkata Subba Rao Jampani, Dirk J. Mulder, Kevin Reguengo De Sousa, Anne-Hélène Gélébart, Jan P. F. Lagerwall,\* and Albertus P. H. J. Schenning\*

Micrometer-scale liquid crystal network (LCN) actuators have potential for application areas like biomedical systems, soft robotics, and microfluidics. To fully harness their power, a diversification in production methods is called for, targeting unconventional shapes and complex actuation modes. Crucial for controlling LCN actuation is the combination of macroscopic shape and molecular-scale alignment in the ground state, the latter becoming particularly challenging when the desired shape is more complex than a flat sheet. Here, one-step processing of an LCN precursor material in a glass capillary microfluidic set-up to mold it into thin shells is used, which are stretched by osmosis to reach a diameter of a few hundred micrometers and thickness on the order of a micrometer, before they are UV crosslinked into an LCN. The shells exhibit radial alignment of the director field and the surface is porous, with pore size that is tunable via the osmosis time. The LCN shells actuate reversibly upon heating and cooling. The decrease in order parameter upon heating induces a reduction in thickness and expansion of surface area of the shells that triggers continuous buckling in multiple locations. Such buckling porous shells are interesting as soft cargo carriers with capacity for autonomous cargo release.

## 1. Introduction

Responsive soft matter is a growing field in materials science. The controlled morphological changes of a material in response to an environmental variation is of interest not only from a fundamental physics and chemistry point of view,<sup>[1]</sup> but also in many applied fields such as biomedical devices,<sup>[2]</sup> microfluidics,<sup>[3]</sup> or soft robotics.<sup>[4]</sup> To achieve controlled deformation, a number of materials classes have been proposed as actuators, such as nanocomposites, dielectric elastomers, hydrogels, and polymerized liquid crystals.<sup>[5,6]</sup> Mirvakili and Hunter recently presented an overview of various research fields which are in the line of developing artificial muscles, giving rich examples of potential applications of artificial actuators, as well as of the challenges encountered.<sup>[6]</sup> Here, we focus on liquid crystal-based actuators, among which liquid crystal networks (LCNs) play a dominant role. Provided that the mesogens

(liquid crystal-forming molecules or moieties) can be aligned in a controlled fashion, the desired deformation can be programmed, since the relation between mesogen orientation and actuation motion can be predicted. Many studies reporting on LCN-based actuators have been carried out, where the trigger can either be electricity,<sup>[7]</sup> humidity,<sup>[8]</sup> light,<sup>[9,10]</sup> pH,<sup>[11]</sup> or temperature.<sup>[12]</sup>


The majority of LCN-based actuators are made as flat films, largely because of the key role of the mesogenic alignment (represented by the *director*,  $\mathbf{n}$ , the preferred orientation of the mesogen main symmetry axis) in determining the actuation motion and the fact that the technology for controlling the director field  $\mathbf{n}(\mathbf{r})$  as a function of location  $\mathbf{r}$  is best developed for flat films. A free-standing LCN film can be unidirectionally stretched to promote mesogen alignment along the stretching direction.<sup>[13]</sup> Alternatively, if a liquid LCN precursor mixture is filled into the narrow space between two parallel rigid substrates (a 'cell') holding tailored aligning layers, these can pattern even highly complex  $\mathbf{n}(\mathbf{r})$  across the surface, prior to polymerization and crosslinking.<sup>[10,12]</sup> While this latter technique can lead to advanced actuation modes, a challenge is that the confining substrates have to be removed from the LCN without damaging it. Director fields of intermediate complexity have also been programmed into LCNs using a radial magnetic field.<sup>[14]</sup> All these approaches share the restriction that the LCN in its ground state has the shape of a flat film.

Dr. V. S. R. Jampani, K. R. De Sousa, Prof. J. P. F. Lagerwall  
Physics and Materials Science Research Unit  
162a Avenue de la Faiencerie L-1511, Luxembourg  
E-mail: jan.lagerwall@lcsoftmatter.com

Dr. D. J. Mulder, Dr. A. H. Gélébart, Prof. A. P. H. J. Schenning  
Laboratory of Stimuli-responsive Functional Materials and Devices  
Chemical Engineering and Chemistry  
Eindhoven University of Technology  
P.O. Box 513, 5600 MB, Eindhoven, The Netherlands  
E-mail: a.p.h.j.schenning@tue.nl

Dr. D. J. Mulder  
Dutch Polymer Institute (DPI)  
P.O. Box 902, 5600 AZ, Eindhoven, The Netherlands

Dr. A.-H. Gélébart, Prof. A. P. H. J. Schenning  
Institute for Complex Molecular Systems (ICMS)  
Eindhoven University of Technology  
P.O. Box 513, 5600 MB, Eindhoven, The Netherlands

 The ORCID identification number(s) for the author(s) of this article can be found under <https://doi.org/10.1002/adfm.201801209>.

© 2018 The Authors. Published by WILEY-VCH Verlag GmbH & Co. KGaA, Weinheim. This is an open access article under the terms of the Creative Commons Attribution-NonCommercial-NoDerivs License, which permits use and distribution in any medium, provided the original work is properly cited, the use is non-commercial and no modifications or adaptations are made.

DOI: 10.1002/adfm.201801209

Moving away from the conventional flat family of LCN actuators, recent studies have described the fabrication of LCN particles with spherical topology (the shape is often ellipsoidal), typically produced at high throughput using microfluidic pathways.<sup>[15–17]</sup> In the pioneering example of Ohm et al.,<sup>[17]</sup> silicone oil was used as the continuous phase, convenient but with strong restrictions on the options to control the LC alignment by using surfactants (the large majority of which are designed for aqueous hosts). Instead, the alignment was so far controlled by the rotational shear flow of the LCN precursor liquid within the silicone oil continuous phase, the polymerization and crosslinking being done using rapid UV curing during production. Another study used post-droplet production stretching within a sacrificial polymer matrix.<sup>[18]</sup> The spherical actuators present the advantage that no substrates need to be removed after LCN production, that many identical LCN particles can be produced in a short period of time with minimum loss of material (provided a fully optimized process), and that the topology of a self-closing surface imposes interesting conditions on the director field, the exact situation depending on whether the director is parallel or perpendicular to the boundary of the particle.<sup>[19]</sup> Moreover, the self-closing topology together with the small size means that reproducible alignment can happen on its own, by liquid crystal self-organization, in particular if the sphere is hollow, i.e. a spherical shell rather than a drop.<sup>[15]</sup>

The interest in liquid crystal shells has been steadily increasing in the past years and the fundamental understanding has been pushed quite far.<sup>[19,20]</sup> They constitute a stimulating tool for fundamental research in spontaneous ordering in soft matter and some application opportunities have been proposed, as photonic elements,<sup>[21]</sup> for generating unclonable security patterns,<sup>[22]</sup> in sensing<sup>[23]</sup> and—in case of LCN shells—as soft actuators.<sup>[15]</sup> By using a microfluidic set-up to form the shells, their dimensions can be controlled in a precise way. The production method allows for the choice of different inner and outer fluids, which subsequently will determine the director alignment in the shell. Yet, the delicate nature of the liquid–liquid interfaces bounding regular LC shells represents a drawback, limiting their lifetime and preventing their removal from the continuous liquid phase. To circumvent this limitation, some reports have included mesogens with polymerizable end groups, either for polymer stabilization of a shell that remains largely fluid<sup>[24]</sup> or for turning the shell into a polymeric solid or rubber.<sup>[15,25]</sup> So far, only one study was presented with LCN shell actuators.<sup>[15]</sup> These had biaxial ellipsoidal shape at room temperature and elongated along one short axis upon heating. While this provided a proof of concept, the shells were relatively large and thick, and the control of alignment was modest. This was largely because the production procedure locked in the flow-induced alignment during microfluidic production. A better alignment and greater tunability of thickness and diameter can be expected if the LCN precursor material is given enough time between shell production and crosslinking to rearrange  $\mathbf{n}(\mathbf{r})$  into a configuration that minimizes the free energy in the shell. It is the aim of this work to explore this conjecture.

Herein, we report the first example of LCN shell soft actuators in which the crosslinking was carried out at steady state, after the microfluidic shell production, using aqueous

inner and outer fluids. We employ main-chain LC oligomers dissolved in an isotropic solvent for production, giving advantages over many commonly used low molar mass reactive mesogens, in particular a shift of the processing window of the shells to or close to room temperature. The crosslinking takes place after shell formation, solvent removal and osmosis, locking into place the liquid crystalline order spontaneously developed by the oligomers, guided by their interaction with the surrounding aqueous fluids. The shells turn out to be very thin, porous, and with homeotropic alignment. Upon heating, the shells exhibit a remarkable buckling behavior, continuous and reversible on cooling.

## 2. Results

### 2.1. Synthesis and Characterization of the Reactive Mesogenic Oligomer

In order to obtain a viscoelastic nematic reactive mesogen that can be used for the fabrication of shells from solution we prepared a relatively short acrylate main-chain oligomer. Such a nematic LC oligomer will have sufficient mobility to allow spontaneous surface alignment and suppress crystallization after shell preparation and solvent extraction. After alignment of the oligomeric mesogens in the shell, the acrylic end-groups can be UV photo-crosslinked to obtain elastomeric polymer shells. The main-chain LC oligomer (**oligomer 1**) was prepared by thiol-ene addition of the mesogenic diacrylate RM82 and dithiols 3,6-dioxa-1,8-octanedithiol (DODT) following the procedure of Gélébart et al.,<sup>[26]</sup> see **Figure 1**. RM82 was present in slight excess to obtain an oligomer with acrylate end groups, enabling crosslinking into an LCN at a later stage. With gel permeation chromatography, we determined the number average molecular weight ( $M_n$ ) of the resulting oligomer to be approximately 5800 g mol<sup>−1</sup> with a polydispersity index ( $M_w/M_n$ ) of about 2.5. The presence of acrylate end-groups was confirmed by FTIR measurements and <sup>1</sup>H-NMR indicated a degree of polymerization of 7–8, see Supporting Information (SI).

The phase behavior of **oligomer 1** was studied by differential scanning calorimetry (DSC), revealing a clearing point of 87 °C, glass transition at  $T_g \approx -21$  °C and one inter-mesophase transition at 49 °C (Figure S2a, Supporting Information). The nature of the two mesophases in the uncrosslinked oligomer was judged by polarizing optical microscopy (POM) texture analysis (details in SI) to be nematic and smectic, respectively. As control to the shell actuators, free-standing flat polymer films (50 μm thick, uniform in-plane alignment) were studied first. A mixture of **oligomer 1** and 0.5 wt% photoinitiator (Irgacure 819) was filled in the molten state into a standard LC cell with rubbed polyimide aligning layers. After UV crosslinking, opening of the cell and removal of the crosslinked film from the substrates, the thermal behavior of the network film was studied by DSC (see Figure 1a). The glass transition temperature was increased to −12 °C compared to the pristine oligomer. In the first heating curve, a broad peak centered at 68 °C was observed. This might indicate that after crosslinking the

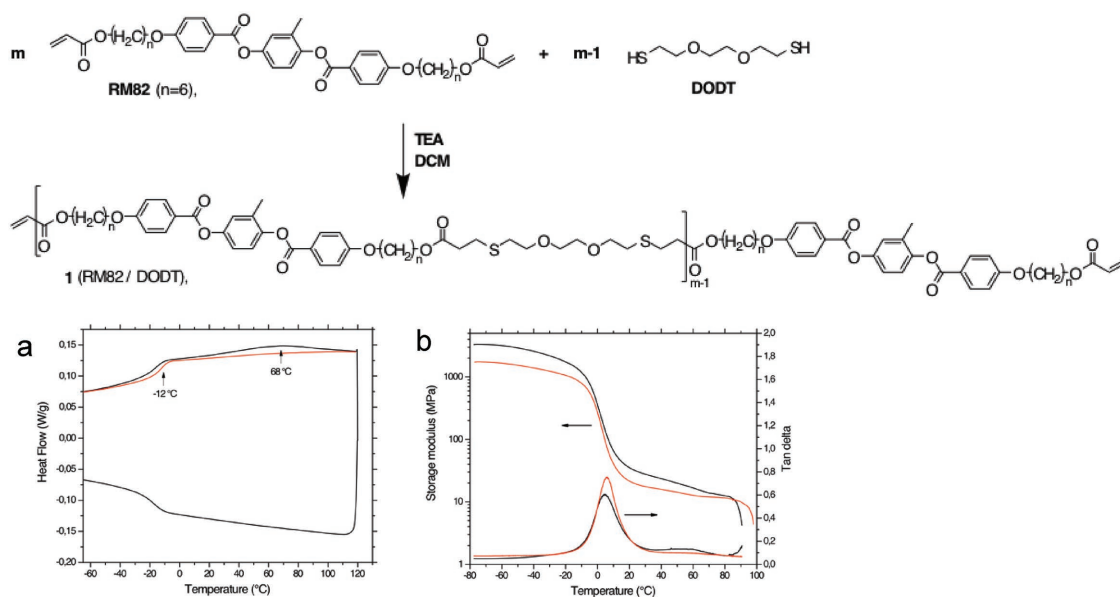


**Figure 1.** Synthetic route of the thiol-ene Michael addition reaction to obtain **oligomer 1** (details in the SI). Thermal and mechanical properties of surface aligned free standing LCN films. a) DSC thermogram. The black curve shows the first heating and cooling cycle and the red curve is from the second heating. b) DMTA thermogram of the LCN. The black and red curves represent the storage modulus and  $\tan \delta$ , parallel, and perpendicular to  $\mathbf{n}$ , respectively.

polymer slowly crystallizes at room temperature. No other phase transitions were detected, indicating that the nematic LC phase was locked in the polymer network. Dynamic mechanical thermal analysis (DMTA) of the film in the glassy state showed a storage modulus ( $E'$ ) plateau at about 2 GPa. On heating, a steep drop in  $E'$  was observed at  $T_g$ . Above  $T_g$  (from 20 to 90 °C),  $E'$  reaches a rubbery plateau of about 10 MPa. The  $\tan \delta$  curve suggests another transition at about 60 °C which might be attributed to melting of crystallites in the sample. The storage modulus parallel to the alignment ( $E'_{\parallel}$ ) was found to be between 1.9 (glassy state) and 1.3 (rubber state) times higher than perpendicular ( $E'_{\perp}$ ).

## 2.2. LCN Shells Produced by Glass Capillary Microfluidics

Shells of an isotropic solution of **oligomer 1** in dichloromethane (DCM) are produced using a glass capillary microfluidic device following the basic design principle of Utada et al.,<sup>[27]</sup> see **Figure 2a**, with details specific to our set-up given in the SI. Since we are working with a minimal amount of starting material (400 mg of **oligomer 1** in 1600 mg of DCM), the time frame of the experiment is too short to achieve true flow stabilization, hence the shells are more polydisperse than typical for microfluidic shell production. The produced shells are collected in the same glycerol–water solution of polyvinyl alcohol (PVA) as used for production, followed by a multi-step dilution with fresh water (see SI). This process allows DCM to diffuse away from the shells, slowly taking them through the transition from isotropic to nematic, as witnessed by birefringence emerging in the shells early in the process. Already at this stage, the texture reveals a radial alignment of the director, i.e. the shells develop with homeotropic alignment, which remains until they are crosslinked into LCNs.

The dilution of the outer phase commences 1 h after shell production. From this moment on, the liquid state shells are undergoing an osmotic expansion,<sup>[28]</sup> gradually making the shells larger and thinner, because the solute concentration inside the shell is greater than in the diluted external phase. Moreover, the inner phase is denser than the diluted external phase, hence the inner droplet sinks towards the bottom, making the shells substantially thinner at the bottom than at the top throughout the osmosis stage. We subject shells to osmosis for times varying from 24 to 72 h, ending the process by irradiating the shells with UV light in order to initiate the crosslinking of **oligomer 1**, changing their state from liquid to that of a polymer network. The director field retains its initial homeotropic alignment throughout the procedure, the quality improving with osmosis time. By crosslinking the shells, this configuration is permanently locked in. Throughout the process, the shells are kept at about 50 °C, ensuring that the shells enter the nematic state as the DCM is removed and keeping the viscosity sufficiently low to promote the overall alignment into an energy-minimizing configuration.

To confirm the homeotropic director configuration in the final LCN shells, they are investigated in the polarizing microscope, see **Figure 2d–f**. Here, four shells of varying diameter but similar thickness are shown without analyzer (d), between crossed polarizers (e), and between crossed polarizers with a first-order wave plate inserted (f), respectively. In the latter case, the optic axis of the wave plate runs in the SW–NE direction, as indicated by the line labeled  $\lambda$  in **Figure 2f**. The osmosis process has made the shells extremely thin, on the order of a micrometer after 24 h osmosis (see below), the 72-h osmosis shells in **Figure 2** expected to be even thinner. This is in stark contrast to the earlier produced LCN shells, which had thickness on the order of 100  $\mu\text{m}$ .<sup>[15]</sup> The black cross with bright corners and the lack

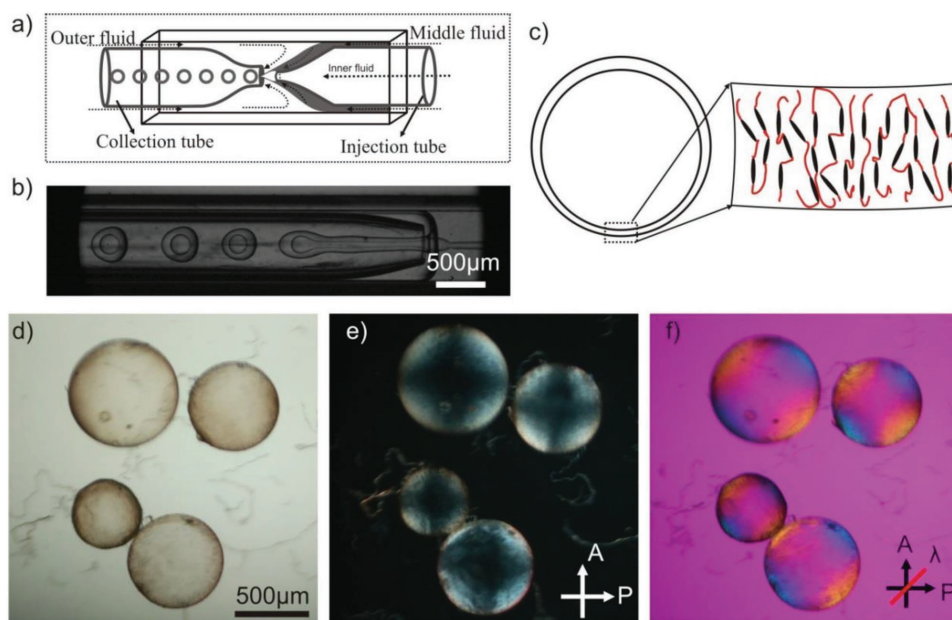


**Figure 2.** a) Schematic view of a glass capillary-based microfluidic set-up for shell production. b) A snapshot shows the LCN precursor mixture encapsulating the inner phase of water/glycerol/PVA solution and flow along with outer phase of water/glycerol/PVA solution. Note that the shells are not uniform in size during production. c) Schematic illustration of cross-sectional view of homeotropically aligned LCN shell. The red colored lines indicate folded oligoethyleneglycol spacers which might effectively promote homeotropic alignment. d–f) The microscope images of LCN shells prepared with 72 h of osmosis prior to crosslinking, taken in bright field mode (d), between crossed polarizers (e), and between crossed polarizers with a wave plate inserted (f), respectively.

of topological defects in the textures in Figure 2d–f are clear signs of homeotropic alignment, and confirm that the shells are neither planar-nor hybrid-aligned.<sup>[19,29,30]</sup> Indeed, the alternation of blue and yellow colors appearing with first-order  $\lambda$  plate confirms that the projection of the director is oriented in the apparent radial direction, as expected for homeotropic-aligned shells. While the birefringence textures of the homeotropic non-elastomeric nematic shells in refs.[29,30] had multiple rings overlaid on the cross, indicating that they covered some three orders of interference, we notice that no ring is visible in Figure 2e. The corners here barely reach the grey-white area of the Michel–Lévy chart. We attribute this to the exceptionally thin shells resulting from the long osmosis process, the shell thickness being an order of magnitude lower than in the mentioned reference works on low molar mass homeotropic LC shells.

Even after crosslinking, all our LCN shells are permeable to water and subject to osmosis, should a concentration gradient exist across the shell wall. To demonstrate this, we conduct an experiment where we set-up the osmotic pressure in the opposite direction compared to the production conditions (details in SI). Prior to crosslinking, the shells had been subject to osmotic expansion for about 24 h. By transferring a suspension of these LCN shells to an 8 M aqueous solution of  $\text{CaCl}_2$ , we trigger a strong outwards-directed osmotic flow of the liquid inside the shell, which now has a much lower solute concentration than the outside. This results in drastic shell shrinkage and eventually a complete collapse onto the substrate, as shown in Figure S3 of the SI. The permeability suggests that our shells are highly porous, a conjecture that is confirmed below.

### 2.3. Thermal Actuation of LCN Shells

The LCN shells, suspended in pure water, are transferred to a rectangular glass capillary which is inserted in a hot stage mounted on a POM, for thermal actuation tests with video monitoring. Upon heating (here at the fast rate of  $30 \text{ K min}^{-1}$ ), the LCN network relaxes towards a more random configuration, as confirmed by a decreasing birefringence  $\Delta n$ , see Figure 3A–E/i–v. The standard model of LCN actuation predicts a shrinkage along the original director and expansion in both perpendicular dimensions. For the homeotropic shell, we should thus expect a reduction of shell thickness and expansion of the surface area, the latter then requiring an increase in shell radius and volume contained within the shell. In a shell that is fully permeable to water this would, therefore, lead to an influx of liquid from the outer phase, in order to accommodate the internal volume increase. However, in our heating experiments, we see only a minor change in radius and instead the LCN shells start buckling, developing indentations at  $65^\circ\text{C}$ , see Figure 3b/ii. The number of indentations increases upon further heating. All indentations relax back in the reverse sequence when cooling back to the starting point, as shown in Figure 3f–j/F–J/vi–x. The continuous thermal actuation sequence of the shells follows the trend of the continuously decreasing  $E'$  measured for the flat film (see Figure 1b). However, a comparison between the flat film and shells is not straightforward, since in the latter case, we additionally have the surrounding aqueous phase, a significant porosity, as well as the spatially varying thickness of the shell (see Discussion).

The buckling could be repeated many times without any fatigue (see Figure S4 and Videos 1, 2, and 4 in the SI),



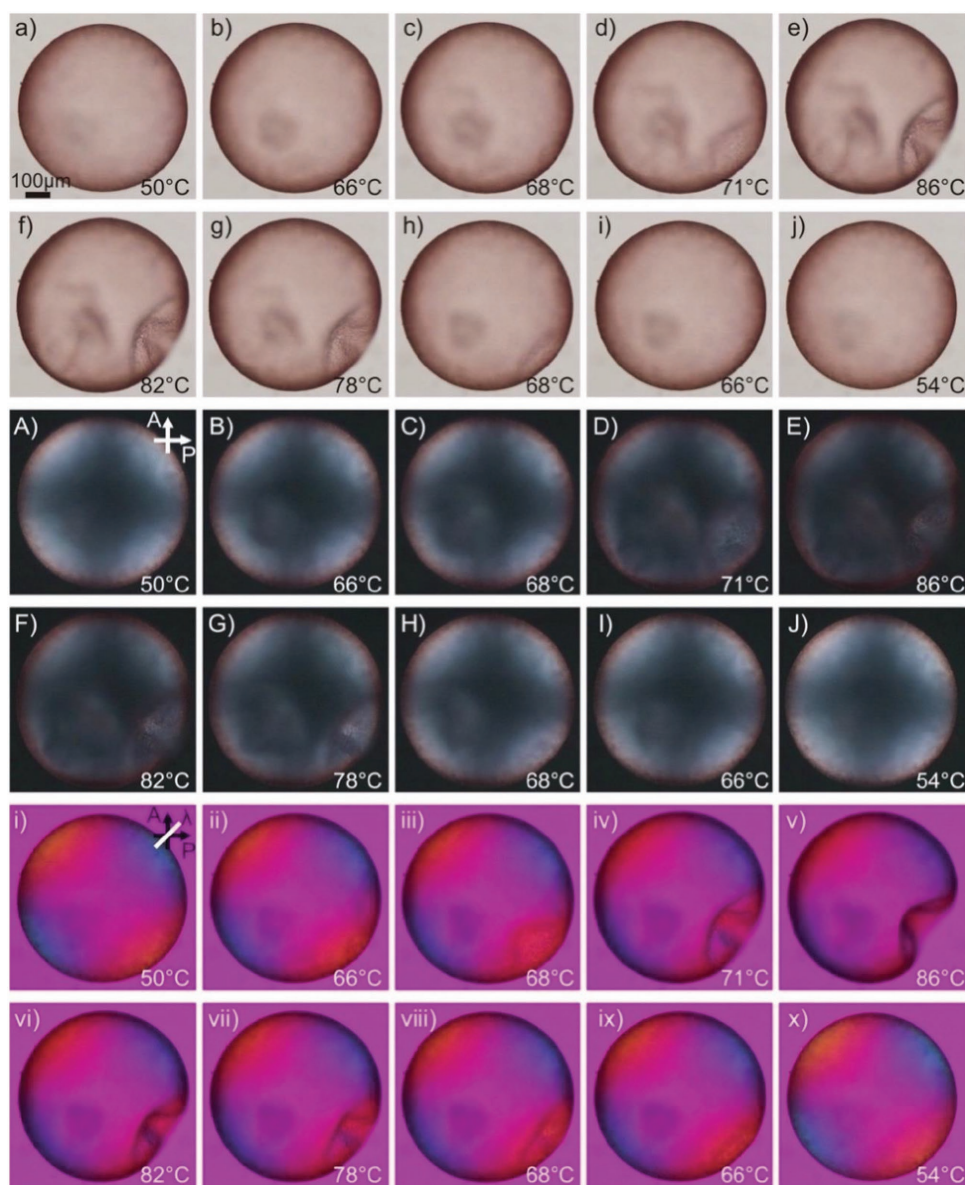


**Figure 3.** a–j) Snapshots of an LCN shell actuator (prepared with 72 h of osmosis prior to crosslinking) during heating and cooling cycles ( $30 \text{ K min}^{-1}$ ). Several indented regions sequentially develop at different temperatures as the shell is heated. A–J) Analogous snapshots between crossed polarizers, and i–x) with a first-order  $\lambda$  phase plate inserted. As evidenced by the expansion of the black cross in parts (A–E), the overall birefringence of the shell decreases upon heating. It increases back to its original state upon cooling (F–J).

revealing that the indentations always appear/disappear in the same locations and in the same sequence, with small hysteresis. The high-temperature change rate during the experiment of Figure 3 does result in some apparent hysteresis, but this is mainly due to the thermal inertia of the system. The fully reversible LCN shell actuation results in the recovery of the homeotropically aligned spherical shape at the end of the cooling cycle, as confirmed also by the original birefringence. The repeatable and largely hysteresis-free buckling sequence suggests that subtle local variations in shell character define where indentations occur and at what temperature. Moreover, the continuity of the process means that we can keep the shell in an intermediately buckled state as it is for a long time

(at least for 30 min duration) by maintaining constant temperature. This can be seen Videos (5–7) in the SI. Such a stable (partially) actuated state, requiring no continuous energy input to the actuator, corresponds to the catch state discussed by Mirvakili and Hunter.<sup>[6]</sup>

To probe the shell with more detail at different stages of actuation, we study a shell that has been doped with a fluorescent dye using fluorescent confocal polarization microscopy (FCPM). Also this shell was produced with 72 h of osmosis prior to crosslinking. Its spherical shape at room temperature and its increasingly indented shape at two elevated temperatures are shown in Figure 4. The FCPM imaging reveals the porous nature of the shell and also that the surface profile is

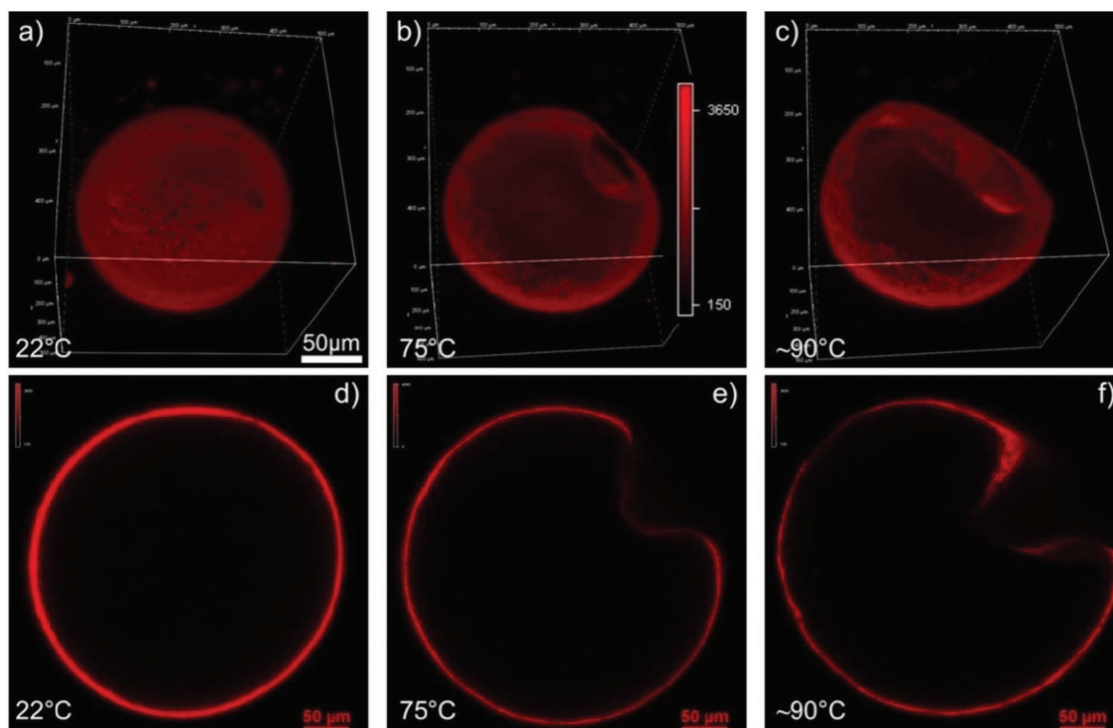


**Figure 4.** a–c) Three-dimensional image of an LCN shell (produced with 72 h osmosis prior to crosslinking) taken using FCPM during heating. The pronounced indented regions at 75 °C and 90 °C are seen. d–f) The equatorial cross-section of the LCN shell is imaged at 22 °C, 75 °C, and 90 °C, respectively.

not uniform. As shown in Figure 4a, some regions appear to have substantially larger pore size than others (see also Videos 3 and 4, SI). The pattern of pores reminds of spinodal decomposition patterns, suggesting that microphase separation during the process of extracting the DCM solvent may have promoted the pore formation. While we cannot exclude that some phase separation between dye and LCN took place in the shells prepared for FCPM, which would yield darker patches without actual holes, the strong evidence for pores from the osmosis experiments as well as from regular POM, and the fact that the shell overall shows rather uniform fluorescence, suggest that the dark areas are indeed gaps in the LCN.

Comparing shells that underwent different times of osmosis (from 24 to 72 h), we find that the pore size increases with osmosis time. The longest osmosis time yields shells with pores that are easily visible by optical techniques, whereas shells produced with only 24 h osmosis appear intact in optical microscopy (Video 1, SI). However, electron microscopy (see below) reveals that also these shells have a great number of small pores. Interestingly, all shells, regardless of osmosis time, show similar indentation behavior (compare Videos 1, 2, and 8, SI). This suggests that the pores do not have a major impact on the mode of actuation.

While it would be informative to have quantitative data on shell thickness and surface area at different stages of actuation, this is challenging to obtain. We can, however, obtain a rough estimate at least of the change in shell thickness by studying the fluorescence signal in the cross-sectional FCPM images in Figure 4d–f, as plotted in Figure 5. The absolute thickness values are clearly overestimated with this method (see below for

better absolute data on another shell from electron microscopy), but we may consider the relative change in apparent shell thickness as representative of the relative change in physical thickness in a first rough approximation. Within this interpretation, the FCPM data suggest a roughly threefold thickness decrease upon heating, as the apparent thickness decreases from about 12  $\mu\text{m}$  in the original spherical state to about 4  $\mu\text{m}$  in the final

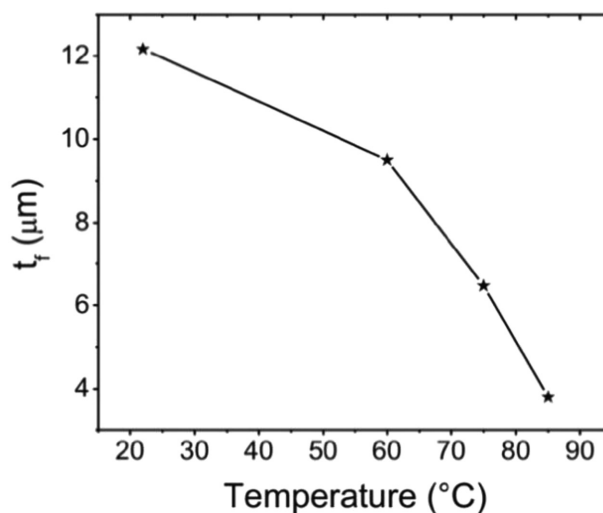


**Figure 5.** The apparent wall thickness  $t_f$  of the shell in Figure 4, as judged from the fluorescence (f) signal, as a function of temperature. Note that the absolute values are much larger than the real shell thickness, and also the relative change is most likely an overestimate.

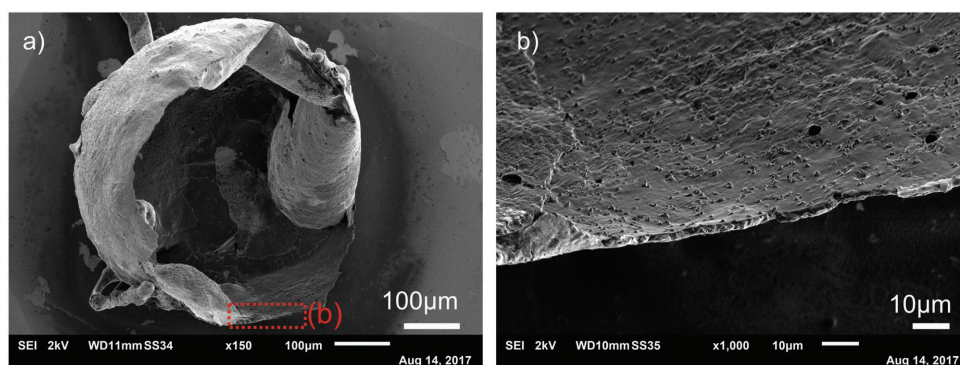


**Figure 6.** SEM images of a shell (coated with about 25 nm of gold) produced with 24 h osmosis prior to crosslinking, fractured by sonication. a) Image of the entire shell with folded regions of the shell wall. b) Close-up at the bottom of the shell shown in part (a), allowing the wall thickness to be measured rather accurately.

buckled state. We emphasize that these numbers are very rough approximations, overestimating the response since the change in order parameter should influence the dye fluorescence and thus the apparent shell thickness. Nevertheless, we expect a considerable increase in shell surface area upon actuation, although the total volume may decrease somewhat, as for normal polymer networks upon heating.

Finally, to get a reliable measure of the absolute shell thickness, we investigate shells using scanning electron microscopy (SEM). The LCN shells are soft and thin, leading to smearing of the shell when cutting with a scalpel (see Figure S5, SI). To measure the shell thickness and characterize the surface topography, we therefore instead tear some LCN shells apart prior to imaging, by ultrasonication of the suspension for 1 min. This method is relatively robust, yielding a few shells with large holes. Imaging the broken shell wall, we can estimate the shell thickness at different locations, finding an average value of about 1.5  $\mu\text{m}$  for the shell shown in Figure 6, which was subject to about 24 h of osmosis prior to crosslinking. While the lack of shell monodispersity during production (see Figure 2 and corresponding text) prevents us from applying this result to other shells, this is still an order of magnitude less than the thickness estimated from the fluorescence signal in the FCPM study of a shell that was subject to three times as long osmosis. This suggests that the optical investigation cannot yield reliable absolute values concerning the shell thickness. Note that all our shells still possess glycerol and PVA inside the shell volume even after the crosslinking. The PVA may play a role in suppressing pore visibility under SEM and it may also influence the inward flux of water during actuation.

### 3. Discussion

Thermotropic nematics often develop planar alignment in water contact,<sup>[29,31]</sup> hence the homeotropic alignment of our LCN shells is somewhat surprising, reminding more of what can be seen with smectic LCN droplets.<sup>[32]</sup> Since the homeotropic orientation was present as soon as the nematic phase started developing, it is not a result of the network formation during crosslinking. Two other factors may play a role. First, the osmotic flow of water through the liquid shell into the

inner droplet is radial, which could promote the radial molecule alignment of a homeotropic shell. Second, the chemical design of the oligomers may promote radial alignment, as the oligoethyleneglycol spacers are considerably more hydrophilic than the mesogens. The oligomers are likely to take on a folded conformation within the shell, running back and forth preferentially in the radial direction with the ethyleneglycol parts making the interface to the aqueous phases, as illustrated in the cartoon in Figure 3c.

Throughout the course of this study, we have produced and investigated hundreds of shells, all developing homeotropic alignment and all exhibiting reversible buckling inwards upon heating. Buckling of spherical shells is a fascinating phenomenon, normally triggered by a pressure increase on the shell outside and often being irreversible or showing considerable hysteresis.<sup>[33]</sup> The buckling of our porous LCN shells is clearly quite different. Beyond the fundamental scientific interest, sphere buckling can also be a useful tool, for instance as a means to direct colloid aggregation by creating indentations in large spheres with a geometric fit to smaller spheres.<sup>[34]</sup> Our LCN shells constitute an interesting new system, as the buckling is not induced by changes in the environment but by a change in the shell itself. If it were not for the pores, the observed buckling would naturally be attributed to the effective external pressure (or internal suction) that would arise as the shell is trying to expand around an internal fluid that cannot increase its volume. However, the experiments described above give clear evidence of the fact that all shells are porous, in the case of long osmosis time very much so. This means that liquid should easily flow through the shell to accommodate any change in surface area that the shell desires, with the consequent change in internal volume and without any buckling, yet we always see a shell radius that is close to constant, coupled with considerable buckling during actuation.

We currently consider two possible origins of the porosity. 1) Polymerization starts while there is still a small amount of DCM solvent in the shell, separating out as droplets, for instance via spinodal decomposition. Because these droplets do not contain (sufficient) reactive species, they will create pores in the network as it forms upon UV polymerization. 2) First the whole shell is crosslinked into a pore-free state but then subject to further osmotic stretching, to the extent that the sheet ruptures



in some places, creating the pores via a cavitation process. We currently favor option (1), but we do not rule out any scenario at this point.

The FCPM investigations reveal that at least the shells that underwent long osmosis are strongly heterogeneous, with some regimes having much larger pores than others. However, the fact that the buckling behavior is essentially the same for 24 or 72 h of osmosis suggests that the variation in pore size with osmosis time, and indeed with location within a single shell, may not be the key factor to explain the buckling. The local variations in pore size are most likely a result of the highly asymmetric shell geometry during osmosis, with the thin bottom compressed by the dense inner droplet letting through liquid from the outer to the inner phase easier than the thick top. Likewise, the DCM solvent should escape easier from the thinnest part of the shell than from the thickest part. We expect this asymmetry during osmosis to give rise to, not only varying pore size, but possibly also a non-uniform character of the LCN itself. Further studies are needed to confirm this, but one notes that the difference in cross-section area between shell in and outside, due to its curvature, as well as the unidirectional flow of liquid from the outside to the inside during osmosis, both break the symmetry between the two shell interfaces.

One may thus speculate that mesogen density, degree of order and/or crosslink density may be different on the two sides. Each of these asymmetries would give rise to local variations in actuation efficiency, a weak network or low-order parameter yielding poor actuation. If a radial variation would exist in one or several locations, such that the shell inside tends to actuate stronger than the shell outside, we would have the same situation as in a bimetal switch, where reversal of curvature, as in shell buckling, happens beyond a threshold expansion of the more responsive side. However, a striking difference to this type of discrete 'snap-through' buckling, as is also typical in regular pressure-driven buckling of shells once the threshold pressure is reached,<sup>[33]</sup> is that the buckling in our shells is soft and continuous, allowing us to stop at any point in the process. The particular degree of buckling is left stable, as shown during the FCPM investigation in Figure 4. This may be due to the shell asymmetry, as it is known that buckling may follow a very different behavior in asymmetric shells compared to symmetric ones, with less or no hysteresis and reduced 'snap through'.<sup>[33]</sup>

We believe that the buckling of our shells is not driven by a pressure difference, as in ordinary shell buckling, but is rather dictated by the particular structural variations within the LCN shell that are a result of how the shells were produced. Since the shell is porous, actuation cannot build-up a pressure difference. It will, however, promote mixing of the inner and outer fluids, potentially useful for controlled delivery applications. While the similarity in actuation for shells exhibiting short and long osmosis suggests that the porosity does not have major impact on the mode of actuation, we expect that the pores still influence the response. In fact, there are theoretical as well as experimental demonstrations that holes in a shell can strongly affect the buckling behavior,<sup>[35]</sup> although the area fraction of holes in these studies was much greater and the hole size was constant and the distribution spherically symmetric. To the best of our knowledge the effect of a spatial variation of hole density and/or size, as in the case of our LCN shells, has not yet been investigated.

## 4. Conclusions

We have demonstrated that thin buckling LCN shells can be produced reliably in a microfluidic pathway, starting from a photo-crosslinkable LC oligomer dissolved in a solvent. The osmosis-driven expansion and alignment of the LCN precursor shell is a robust method for ensuring homeotropic alignment of the LCN in the shell geometry, probably aided by the amphiphilic design of the oligomer. The shells are porous, most likely linked to the osmosis, as the pore size depends on the osmosis time. It also varies across the shell surface, possibly due to the geometrical shell asymmetry during osmosis. Possibly, pore formation is also promoted by phase separation by spinodal decomposition if some DCM solvent remains in the shells during crosslinking.

Upon heating, the shells actuate by developing a sequence of indentations. The buckling yielding these indentations appears to be continuous and without 'snap-through' character, allowing the process to be stopped at any point by holding the temperature. The actuation, which can be understood as a result of the reduction in order parameter around the radial director, with consequent shell thinning and surface area expansion, is reversible and with little hysteresis, returning the shell back to its original state upon cooling. This comprises an unusual case of buckling of spherical shells that is continuous and requires no pressure difference between inner and outer phases, as it is driven by the thickness and area changes of the shell itself. With future efforts to better control pore formation and alignment control, we envisage that the combination of buckling and partial liquid exchange between inner and outer phases may be useful in active cargo carriers, e.g., for drug delivery.

## 5. Experimental Section

**Materials:** Reactive mesogen compounds, RM82 and RM257 were obtained from Merck KGaA, DODT (95%), PVA (average molecular mass: 13–18 kg mol<sup>-1</sup>, degree of hydrolysis: 87%) from Sigma-Aldrich, triethylamine (99%) from Acros, and Irgacure 819 from Ciba Specialty Chemicals. Nonafluorohexyltriethoxysilane and methoxytriethylenoxypropyltrimethoxysilane (brand name: SIM 6493.4) were purchased from Gelest. All organic solvents used were Analytical Grade and were obtained from Biosolve. 1 M HCl (aq.) was freshly prepared from a 37% HCl solution, Glycerol (Sigma-Aldrich) was added to increase the viscosity in both inner and outer fluids to facilitate the microfluidic production. All reagents were used as received, without further purification. In all the experiments, deionized ultrapure water was used (resistivity: 18 MΩcm, Sartorius Arium pro DI). G205 azo dye for confocal imaging was used.<sup>[36]</sup>

Details on microfluidic shell production, solvent extraction, shell expansion and crosslinking, as well as all characterization techniques, are given in the SI.

## Supporting Information

Supporting Information is available from the Wiley Online Library or from the author.

## Acknowledgements

We thank Robin Selinger and Youssef Mosaddeghian Golestani for valuable discussions. V.S.R.J. and J.P.F.L. acknowledge financial support



from the European Research Council under the European Union's Seventh Framework Programme (FP/2007-2013)/ERC grant agreement number 648763 (consolidator project INTERACT) and Fonds Nationale de la Recherche (FNR, grant ID. C17/MS/11703329/trendsetter). This research of D.J.M. forms part of the research program of the Dutch Polymer Institute (DPI), project 776.

## Conflict of Interest

The authors declare no conflict of interest.

## Keywords

buckling, liquid crystal elastomer actuators, microfluidics, spherical topology

Received: February 14, 2018

Revised: April 20, 2018

Published online: June 5, 2018

- [1] M. Warner, E. M. Terentjev, *Liquid Crystal Elastomers*, Oxford University Press, USA, **2007**, p. 424.
- [2] S. J. Woltman, G. D. Jay, G. P. Crawford, *Nat. Mater.* **2007**, 6, 929.
- [3] A. Sanchez-Ferrer, T. Fischl, M. Stubenrauch, A. Albrecht, H. Wurmus, M. Hoffmann, H. Finkelmann, *Adv. Mater.* **2011**, 23, 4526.
- [4] D. Trivedi, C. D. Rahn, W. M. Kier, I. D. Walker, *Appl. Bionic Biomech.* **2008**, 5, 99.
- [5] L. Hines, K. Petersen, G. Z. Lum, M. Sitti, *Adv. Mater.* **2017**, 29.
- [6] S. M. Mirvakili, I. W. Hunter, *Adv. Mater.* **2018**, 30, 1704407.
- [7] H. Ringsdorf, R. Zentel, *Die Makromol. Chem.* **1982**, 183, 1245.
- [8] a) Y. Liu, B. Xu, S. Sun, J. Wei, L. Wu, Y. Yu, *Adv. Mater.* **2017**, 29; b) L. T. de Haan, J. M. N. Verjans, D. J. Broer, C. W. M. Bastiaansen, A. P. H. J. Schenning, *J. Am. Chem. Soc.* **2014**, 136, 10585.
- [9] a) A. H. Gelebart, D. Jan Mulder, M. Varga, A. Konya, G. Vantomme, E. W. Meijer, R. L. B. Selinger, D. J. Broer, *Nature* **2017**, 546, 632; b) T. Ikeda, M. Nakano, Y. Yu, O. Tsutsumi, A. Kanazawa, *Adv. Mater.* **2003**, 15, 201.
- [10] T. H. Ware, M. E. McConney, J. J. Wie, V. P. Tondiglia, T. J. White, *Science* **2015**, 347, 982.
- [11] L. T. de Haan, V. Gimenez-Pinto, A. Konya, T.-S. Nguyen, J. M. N. Verjans, C. Sánchez-Somolinos, J. V. Selinger, R. L. B. Selinger, D. J. Broer, A. P. H. J. Schenning, *Adv. Funct. Mater.* **2014**, 24, 1251.
- [12] T. J. White, D. J. Broer, *Nat. Mater.* **2015**, 14, 1087.
- [13] a) J. Küpfer, H. Finkelmann, *Macromol. Chem. Phys.* **1994**, 195, 1353; b) J. Küpfer, H. Finkelmann, *Die Makromol. Chem.* **1991**, 12, 717.
- [14] S. Schuhlader, F. Preller, R. Rix, S. Petsch, R. Zentel, H. Zappe, *Adv. Mater.* **2014**, 26, 7247.
- [15] E.-K. Fleischmann, H.-L. Liang, N. Kapernaum, F. Giesselmann, J. P. F. Lagerwall, R. Zentel, *Nat. Commun.* **2012**, 3, 1178.
- [16] C. Ohm, N. Kapernaum, D. Nonnenmacher, F. Giesselmann, C. Serra, R. Zentel, *J. Am. Chem. Soc.* **2011**, 133, 5305.
- [17] C. Ohm, C. Serra, R. Zentel, *Adv. Mater.* **2009**, 21, 4859.
- [18] J. E. Marshall, S. Gallagher, E. M. Terentjev, S. K. Smoukov, *J. Am. Chem. Soc.* **2014**, 136, 474.
- [19] M. Urbanski, C. G. Reyes, J. Noh, A. G. Sharma, V. S. R. Jampani, J. P. F. Lagerwall, *J. Phys.: Condens. Matter* **2017**, 29, 133003.
- [20] T. Lopez-Leon, A. Fernandez-Nieves, *Colloid Polym. Sci.* **2011**, 289, 345.
- [21] a) J. Noh, H.-L. Liang, I. Drevensek-Olenik, J. P. F. Lagerwall, *J. Mater. Chem. C* **2014**, 2, 806; b) Y. Uchida, Y. Takanishi, J. Yamamoto, *Adv. Mater.* **2013**, 25, 3234; c) M. Humar, I. Musevic, *Opt. Express* **2010**, 18, 26995.
- [22] Y. Geng, J. Noh, I. Drevensek-Olenik, R. Rupp, G. Lenzini, J. P. F. Lagerwall, *Sci. Rep.* **2016**, 6, 26840.
- [23] a) R. J. Carlton, J. T. Hunter, D. S. Miller, R. Abbasi, P. C. Mushenheim, L. N. Tan, N. L. Abbott, *Liq. Cryst. Rev.* **2013**, 1, 29; b) J. P. F. Lagerwall, G. Scalia, *Curr. Appl. Phys.* **2012**, 12, 1387.
- [24] J. Noh, B. Henx, J. P. F. Lagerwall, *Adv. Mater.* **2016**, 28, 10170.
- [25] J.-G. Kim, S.-Y. Park, *Adv. Opt. Mater.* **2017**, 5, 1700243.
- [26] A. H. Gelebart, M. Mc Bride, A. P. H. J. Schenning, C. N. Bowman, D. J. Broer, *Adv. Funct. Mater.* **2016**, 26, 5322.
- [27] A. Utada, E. Lorenceau, D. R. Link, P. D. Kaplan, H. A. Stone, D. A. Weitz, *Science* **2005**, 308, 537.
- [28] T. Lopez-Leon, V. Koning, K. B. S. Devaiah, V. Vitelli, A. Fernandez-Nieves, *Nat. Phys.* **2011**, 7, 391.
- [29] J. Noh, K. Reguengo De Sousa, J. P. F. Lagerwall, *Soft Matter* **2016**, 12, 367.
- [30] H.-L. Liang, E. Enz, G. Scalia, J. Lagerwall, *Mol. Cryst. Liq. Cryst.* **2011**, 549, 69.
- [31] J. Brake, N. Abbott, *Langmuir* **2002**, 18, 6101.
- [32] a) H. P. C. van Kuringen, D. J. Mulder, E. Beltran, D. J. Broer, A. P. H. J. Schenning, *Polym. Chem.* **2016**, 7, 4712; b) M. Vennes, R. Zentel, M. Rossle, M. Stepputat, U. Kolb, *Adv. Mater.* **2005**, 17, 2123.
- [33] J. Paulose, D. R. Nelson, *Soft Matter* **2013**, 9, 8227.
- [34] S. Sacanna, W. T. Irvine, P. M. Chaikin, D. J. Pine, *Nature* **2010**, 464, 575.
- [35] a) S. Lin, Y. M. Xie, Q. Li, X. Huang, S. Zhou, *Sci. Rep.* **2015**, 5, 11309; b) J. Shim, C. Perdigue, E. R. Chen, K. Bertoldi, P. M. Reis, *Proc. Natl. Acad. Sci. USA* **2012**, 109, 5978.
- [36] R. Pinol, J. Lub, M. P. Garcia, E. Peeters, J. L. Serrano, D. J. Broer, T. Sierra, *Chem. Mater.* **2008**, 20, 6076.